ACS APPLIED MATERIALS & INTERFACES

Research Article

www.acsami.org

Phosphonic Acid Functionalized Ordered Mesoporous Material: A New and Ecofriendly Catalyst for One-Pot Multicomponent Biginelli Reaction under Solvent-Free Conditions

Malay Pramanik and Asim Bhaumik*

Department of Materials Science, Indian Association for the Cultivation of Science, Jadavpur, Kolkata 700032, India

Supporting Information

ABSTRACT: We report a new ordered 2D hexagonal mesoporous organosilica material (PAFMS-1) bearing phosphonic acid functionality at the surface. This hybrid material showed high Brunauer–Emmett–Teller surface area (565 m^2 g^{-1}) and ordered assembly of mesoporoes with an average pore diameter of ca. 2.1 nm. This novel hybrid mesoporous material has been synthesized via cocondensation of (triethoxysilyl)(propyliminomethyl)biphenylmethyl phosphoester (PEFOS) and tetraethyl orthosilicate (TEOS) in the presence of cationic surfactant cetyltrimethylammonium bromide (CTAB) at 373 K. The phosphoester-functionalized organosilane (PEFOS) precursor has been synthesized for the first time by a simple S_N2 reaction followed by Suzuki coupling and a Mannich reaction. The material has been characterized by powder X-ray diffraction, N_2 sorption, and transmission electron microscopy image analysis, whereas the presence of organic moieties (an aromatic biphenyl ring and an aliphatic side chain), phosphrous, and silicon in the pore wall of the material have been characterized by solid-state magic-angle-spinning NMR, X-ray photoelectron, and Fourier transform infrared (FT-IR) spectroscopic tools. Further, the surface acid strength of the hybrid material has been determined by FT-IR analysis of the samples via temperature-programmed pyridine adsorption studies. The material has been utilized as a reusable heterogeneous catalyst for the synthesis of biologically important and value added multifunctionalized 3,4-dihydropyridin-2-1*H*-(ones)/3,4-dihydropyridin-2-1*H*-(thiones) (DHPMs) through a multicomponent Biginelli condensation reaction under solvent-free conditions at 333 K. The phosphonic acid functionalized 2D hexagonal mesoporous material showed much higher catalytic activity in this multicomponent condensation reaction over sulfonic acid functionalized mesoporous silica (MCM-41-SO_3H) bearing an aliphatic chain in the hybrid framework.

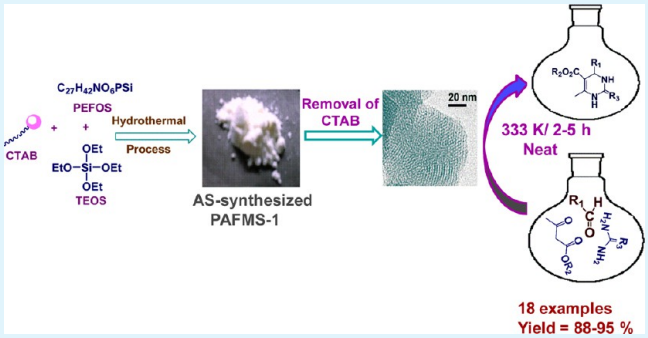

KEYWORDS: *ordered mesoporous material, biphenyl-bridged phosphonic acid, organocatalyst, multicomponent reaction, solvent-free conditions*

INTRODUCTION

One-pot multicomponent reactions (MCRs) have attracted huge research interest in synthetic organic, medicinal, and materials chemistry over the past 2 decades because of the high degree of atom economy and construction of the complex target molecules/frameworks in a convergent way.[1−4] The Biginelli reaction is one of the most important MCRs that offer an efficient route to produce multifunctionalized 3,4-dihydropyridin-2-1*H*-(ones)/3,4-dihydropyridin-2-1*H*-(thiones) (DHPMs) and related heterocyclic compounds through the cycloaddition of aldehyde, 1,3-ketoesters, and urea or thiourea.[5−8] Polyfunctionalized DHPMs have found increasing applications for the synthesis of biologically relevant substances exhibiting a wide range of important pharmacological properties, including mitotic kinesin inhibition, calcium channel modulation, and α_{1a}-adrenergicreceptor antagonism.[9−11] In this context, it is also pertinent to mention that large numbers of multifunctionalized DHPMs have found vibrant therapeutic use for the synthesis of antiviral, antitumor, antibacterial, and antiinflammatory drugs.[12,13] As a consequence, many catalytic methodologies, metal Lewis acids, Brønsted acids or bases, heterogeneous catalysts, and nonconventional techniques, such as microwave, ultrasound, high-pressure, and grindstone chemistry, have been developed to improve the synthesis of this attractive family of compounds.[14−17] However, most of these synthetic methodologies suffer from serious drawbacks like long reaction time, low yield, high reaction temperature, metal leaching, and solubility of the catalyst in the reaction medium.[18−20] Recently, there has been increasing awareness of the right legislation on the maintenance of "greenness" in the catalyst design and catalytic processes, and thus greener reaction pathways and methodologies are highly desirable in

Received: September 30, 2013
Accepted: December 27, 2013
Published: December 27, 2013

the field of chemical and materials research.[21,22] In this context, metal-free organocatalysis is one of the green catalytic methodological approaches in the field of synthetic organic chemistry. However, this strategy faced a lot of practical problems: (1) generally the homogeneous organocatalysts are soluble in a reaction medium and hence are very difficult to separate; (2) various hazardous organic solvents are used as the reaction medium to obtain optimum yield in a given reaction; (3) the reaction time is large; (4) the turnover numbers are low.[23−26] To avoid these problems, the use of a heterogeneous organocatalyst is a smart choice, particularly those that are designed based on functionalized mesoporous silicas because of their high surface area, tunable nanoscale pores, ease of the grafting of organic scaffolds to balance between the hydrophilic and hydrophobic character of the porous architecture, exciting host−guest chemistry, and supramolecular interaction to different extents with the reactant molecules.[27−29]

Herein, we have developed a new synthetic strategy for the design of a biphenyl-bridged phosphonic acid functionalized mesoporous silica (PAFMS-1) with a 2D hexagonal mesoporous framework and its use as an organocatalyst for the convergent one-pot multicomponent Biginelli reaction under solvent-free conditions. Organically functionalized mesoporous silicas have been extensively utilized for the last decade because of their versatile applications in many frontier areas of science like gas storage,[30,31] proton conduction,[32] uranium sequestration,[33] energy transfer,[34] catalysis,[35−37] and collection of toxic ions.[38,39] Recently, we have developed various acid- or base-functionalized mesoporous materials as green, sustainable, and reusable organocatalysts for one-pot MCRs,[40−42] which are highly relevant because of their higher atom economy and bioapplicability of the products. Keeping this idea in mind, we have developed a sulfonic acid functionalized mesoporous material, MCM-41-SO_3H, which is synthesized via mild H_2O_2 oxidation of a 3-(triethoxysilyl)propane-1-thiol-functionalized MCM-41-type material, and used it in the Biginelli reaction as a heterogeneous catalyst under solvent-free conditions at 60 °C for 3 h of reaction time. However, we could isolate only 30 % yield of the Biginelli condensation product using benzaldehyde as the reference aldehyde.[43] Then we changed our strategy to design the catalyst, and we developed PAFMS-1 by simple cocondensation of tetraethyl orthosilicate (TEOS) with the designed phosphoester-containing organosilane precursor molecule (PEFOS, $C_{27}H_{42}NO_6PSi$). The phosphoester-containing organosilica precursor molecule was synthesized by a simple S_N2 reaction and then by Suzuki coupling and followed by the Mannich reaction.[44] The phosphoester moiety in the ordered mesostructured material has been transformed to a corresponding phosphonic acid functionality during hydrothermal synthesis. We used PAFMS-1 as a solid acid catalyst for our targeted Biginelli reaction under solvent-free conditions for 3 h at 60 °C, and we observed an isolated yield of 92 % using benzaldehyde as the reference aldehyde. Now an obvious question arises, why did we use the PEFOS ligand in the pore wall of the silica matrix to catalyze the Biginelli condensation reaction? Here our aim was to synthesis a phosphonic acid functionalized mesopororous silica matrix containing a mobile π-electron system in the pore wall of the material. Hydrophilic phosphonic acid and aromatic ring containing π-electron system will balance between the hydrophilic and hydrophobic character at the pore surface, which is very essential for inclusion of the intermediate charged species of the Biginelli condensation reaction in the porous matrix. Proper arrangements and environments of pores are very essential for diffusion of guest molecules from outside to the mesochannels of the porous materials.[45,46] Keeping this in mind, we aimed to synthesize a phosphoester-functionalized biphenyl-bridged organosilane (PEFOS) precursor molecule and graft it inside the porous silica matrix. Now to prepare our targeted (triethoxysilyl)(propyliminomethyl)biphenylmethyl phosphoester (PEFOS), the simplest way was to use a Suzuki coupling reaction to produce the phosphoester-functionalized biphenyl ring containing an aldehyde group, which is further used to form a Schiff base group by the Mannich reaction. If we had tried to perform both reactions in one pot, then the protons of 4-formylboronic acid would protonate the free amine of (3-aminopropyl)triethoxysilane (APTES), so the chance of a Mannich reaction will decrease largely and we will get protonated APTES as a byproduct. Further, in the purification step, water is needed to remove the palladium source from the reaction medium, but in this condition, a free silane moiety will condense, so our target would not have been fulfilled. So, we have used the two-step process rather one-pot synthesis of the PEFOS molecule. The catalyst can be separated from the reaction mixture by a simple filtration technique and reused eight times without significant loss of its catalytic activity. To the best of our knowledge, this is the first report of a phosphonic acid functionalized mesoporous material in a highly efficient Biginelli condensation reaction under mild reaction conditions.

EXPERIMENTAL SECTION

Materials. Commercially available 4-bromobenzyl bromide, triethyl phosphite, 4-formylbenzeneboronic acid, tetrakis-(triphenylphosphine)palladium(0), and (3-aminopropyl)-triethoxysilane (APTES) were purchased from Sigma-Aldrich. Toluene, tetrahydrofuran (THF), urea, and thiourea were purchased from E-Mark. Various substituted aldehydes were purchased from Avra Chemicals, India.

Synthesis of Phosphoester-Functionalized Organosilane (PEFOS). The final organosilane precursor bearing a phosphoester (PEFOS, $C_{27}H_{42}NO_6PSi$) has been prepared by three-step organic synthesis, as schematically presented in Scheme 1.

Scheme 1. Synthesis of PEFOS

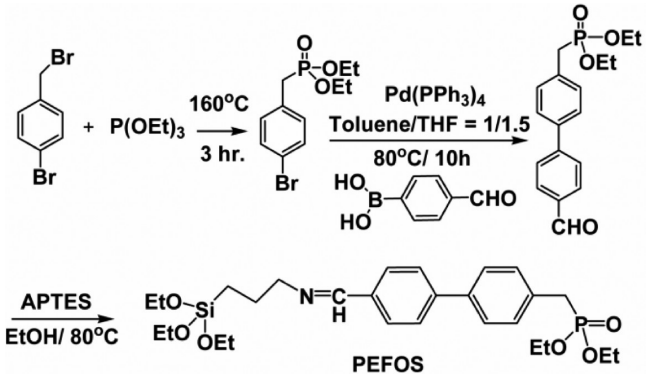

Synthesis of Diethyl(4-bromophenyl) Methylphosphonate via an S_N2 Reaction Pathway. In this typical synthesis procedure, 2.49 g (10 mmol) of 4-bromobenzyl bromide was placed in a 50 mL round-bottom flask fitted with a dropping funnel and a chilled water condenser. The dropping funnel was charged with 2.324 g (14 mmol) of freshly distilled triethyl phosphite [$P(OEt)_3$], and the flask was purged with N_2 gas and heated at 433 K for 3 h. The crude diethyl(4-bromophenyl) methylphosphonate (2.92 g) product was collected by

dx.doi.org/10.1021/am404298a | ACS Appl. Mater. Interfaces 2014, 6, 933−941

vacuum distillation. The crude product was purified by crystallization and characterized by ^{1}H, ^{13}C, and ^{31}P NMR spectroscopy. ^{1}H NMR (500 MHz, $CDCl_3$): δ 7.48 (d, J = 7 Hz, 2H), 7.23 (d, J = 7.5 Hz, 2H), 3.99 (m, 4H), 3.18−3.22 (2H), 1.16 (m, 6H). ^{13}C NMR (500 MHz, $CDCl_3$): δ 132.40, 132.37, 132.32, 131.53, 131.51, 120.21, 61.62, 32.70, 16.49. ^{31}P NMR (500 MHz, $CDCl_3$): δ 26.96 (Figures S1−S3 in the Supporting Information, SI).

Synthesis of 4-Formyl-4′-diethylmethylphosphonato-1,1′-biphenyl via Suzuki Coupling. Now a round-bottom flask attached with a chilled water condenser was charged with diethyl(4-bromophenyl) methylphosphonate (2.8 g, 9.12 mmol), 4-formylbenzeneboronic acid (2.32 g, 15.53 mmol), and sodium carbonate (1.92 g, 18.24 mmol) in water and a toluene/THF (1/1.5) mixture. The whole mixture was homogenized for 1 h under vigorous stirring and heated at 80 °C. Under these synthetic conditions, tetrakis-(triphenylphosphine)palladium(0) (100 mg) was added to the reaction mixture, and heating was continued for another 10 h. After completion of the reaction, 15 mL of water was added to the flask, and the product mixture was extracted with 100 mL of ethyl acetate. The extracted part was thoroughly washed with a water and brine solution and dried over anhydrous sodium sulfate for 1 h. The crude product was collected by vacuum evaporation of the organic fraction. The crude product was purified by silica gel chromatography ($CHCl_3$/MeOH = 10/3) to afford the desired product 4-formyl-4′-diethylmethylphosphonato-1,1′-biphenyl ($C_{18}H_{21}O_4P$) with 58% yield (1.75 g). The compound was characterized by ^{1}H, ^{13}C, and ^{31}P NMR spectroscopy. ^{1}H NMR (400 MHz, $CDCl_3$): δ 9.88 (s, 1H), 7.79 (d, J = 6 Hz, 2H), 7.59 (d, J = 6.4 Hz, 2H), 7.45 (d, J = 6.4 Hz, 2H), 7.29 (d, J = 6.4 Hz, 2H), 3.93 (q, J = 6 Hz, 4H), 3.06−3.10 (2H), 1.14 (m, 6H). ^{13}C NMR (400 MHz, $CDCl_3$): δ 191.37, 146.15, 137.75, 134.87, 131.71, 130.07, 130.14, 129.87, 127.07, 61.73, 33.72, 32.35, 15.80. ^{31}P NMR (400 MHz, $CDCl_3$): δ 26.31 (Figures S4−S6 in the SI).

Synthesis of PEFOS Bearing a Phosphonate Group via the Mannich Reaction. A total of 1.75 g (5.23 mmol) of 4-formyl-4′-diethylmethylphosphonato-1,1′-biphenyl was dissolved into 25 mL of double-distilled dry ethanol placed in a round-bottom flask equipped with a dropping funnel. The dropping funnel was charged with APTES (1.14 g, 5.23 mmol) and 10 mL of freshly distilled dry ethanol. The round-bottom flask was heated at 80 °C, while APTES was added dropwise and heating was extended for 6 h. After completion of the reaction (progress of the reaction was monitored by thin-layer chromatography, TLC), the product PEFOS was a gelatinous liquid and it was collected by vacuum evaporation of ethanol. The compound was characterized by ^{1}H, ^{13}C, and ^{31}P NMR spectroscopy. ^{1}H NMR (400 MHz, $CDCl_3$): δ 8.33 (1H), 7.27−7.78 (8H), 3.95 (4H), 3.72 (6H), 3.54 (2H), 3.28 (2H), 1.68 (2H), 1.12 (15H), 0.58 (2H). ^{13}C NMR (400 MHz, $CDCl_3$): δ 160.70, 132.16, 132.07, 132.00, 131.30, 130.32, 128.95, 127.13, 126.87, 62.19, 61.45, 58.27, 44.9, 18.13, 16.51, 15.42, 6.52. ^{31}P NMR (400 MHz, $CDCl_3$): δ 28.33 (Figures S7−S9 in the SI).

Synthesis of PAFMS-1. In a typical synthetic procedure, 1.50 g of cetyltrimethylammonium bromide (CTAB) and 0.15 g of tartaric acid were dissolved in 25 mL of water and stirred for 1 h at room temperature. Then 2.26 g of tetraethyl orthosilicate (TEOS) was added to this transparent solution for 1 h. Then 1.93 g of PEFOS was dissolved into 5 mL of ethanol and added dropwise to the previous solution (TEOS/PEFOS = 3/1). The mixture was stirred for another 4 h, and the pH of the solution was raised to 12 by a 2 M NaOH solution. The whole mixture was stirred overnight for complete condensation and perfect gel formation. The product was transfered to an autoclave and hydrothermally treated at 373 K for 72 h under static conditions. The light-brown product was collected by filtration, washed several times with distilled water, and dried under vacuum. The surfactant (CTAB) was removed from the as-synthesized material by twice repeating EtOH/HCl extraction, and the resulting material was designated as PAFMS-1 (Scheme 2).

Catalytic Reactions. All of the catalytic reactions were carried out in a two-necked round-bottom flask fitted with a water-cooled condenser and placed in a temperature-controlled paraffin oil bath. In

Scheme 2. Schematic Diagram for Synthesis of PAFMS-1

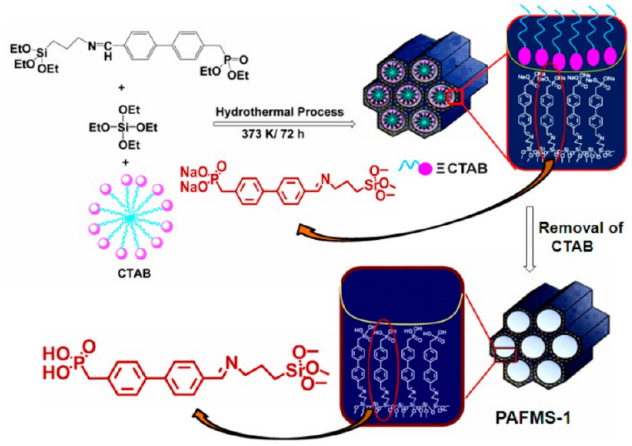

a typical reaction, a 10 mL round-bottom flask was charged with various substituted aldehydes (1 mmol), 1,3-dicarbonyl compounds (1 mmol), urea/thiourea (1 mmol), and 5 wt % catalyst (PAFMS-1) at 60 °C under solvent-free conditions (Scheme 3). The whole reaction

Scheme 3. One-Pot Three-Component Condensation Reaction for the Synthesis of DHPMs Catalyzed by PAFMS-1

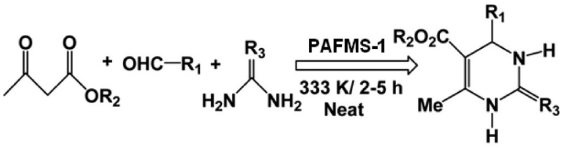

R_1; aryl
R_2; -OEt, -OMe
R_3; O, S

mixture was stirred continuously with a magnatic stirrer for 2−5 h. After conformation of the final products through TLC, the reaction mixture was filtered and washed with ethanol. The crude products were collected by vacuum evaporation of ethanol, recrystallized from ethyl acetate, and washed thoroughly with a brine solution. The combined organic layers thus collected were removed by rotary evaporation under reduced pressure to obtain 3,4-dihydropyridin-2-1*H*-(ones) (DHPMs), which after purification were characterized by ^{1}H and ^{13}C NMR spectroscopic data (see the spectral data in the SI).

Characterization Technique. Powder X-ray diffraction (PXRD) patterns were recorded on a Bruker D-8 Advance diffractometer operated at 40 kV and 40 mA and calibrated with a standard silicon sample, using nickel-filtered Cu Kα (λ = 0.15406 nm). Field-emission scanning electron microscopy (FESEM; JEOL JEM 6700F) was used for determination of the morphology of powder samples. The porous structure was analyzed by high-resolution transmission electron microscopy (HRTEM; JEOL JEM 2010) at an accelerating voltage of 200 kV. N_2 adsorption/desorption isotherms were obtained using a Beckman Coulter SA 3100 surface area analyzer at 77 K under high vacuum. Fourier transform infrared (FT-IR) spectra were recorded using a Nicolet MAGNA-FT-IR 750 series II spectrometer. ^{1}H and ^{13}C NMR experiments were carried out on a Bruker DPX-300 NMR spectrometer. The cross-polarization magic-angle-spinning (CPMAS) ^{13}C NMR and MAS ^{29}Si and ^{31}P NMR spectra were obtained on a 500 MHz Bruker Advanced II spectrometer at a MAS frequency of 8 kHz. X-ray photoelectron spectroscopy (XPS) was performed on an Omicron nanotech operated at 15 kV and 20 mA with a monochromatic Al Ka X-ray source.

dx.doi.org/10.1021/am404298a | ACS Appl. Mater. Interfaces 2014, 6, 933−941

RESULTS AND DISCUSSION

X-ray Diffraction Pattern. The small-angle PXRD pattern of the as-synthesized and template-free PAFMS-1 material is shown in Figure 1. It is seen from the patterns that the small-angle peaks of the as-synthesized material exhibit an ordered 2D hexagonal mesophase, and the ordered mesostructure is also retained in the template-free PAFMS-1 sample. For the as-synthesized material, the most intense peak, observed at 2θ = 2.45°, corresponds to the reflection of the (100) plane (d_{100} = 3.60 nm) of the ordered 2D hexagonal mesophase.[47] The other small peaks were attributed to the reflection of the (110), (200), and (210) planes of the ordered 2D hexagonal mesophase of the material. After removal of the template CTAB molecules from the as-synthesized material, the porous architecture was contracted; consequently, the small-angle diffraction peaks were shifted to slightly higher 2θ values.[48] The estimated d_{100} in the case of template-free PAFMS-1 was 3.2 nm. The corresponding pore diameter was 2.1 nm [calculated from the Brunauer−Emmett−Teller (BET) isotherm and TEM analysis; see below]; hence, the pore wall thickness (D) of the mesoporous material was 1.6 nm [wall thickness $D = (2d_{100}/\sqrt{3})$ − pore diameter].

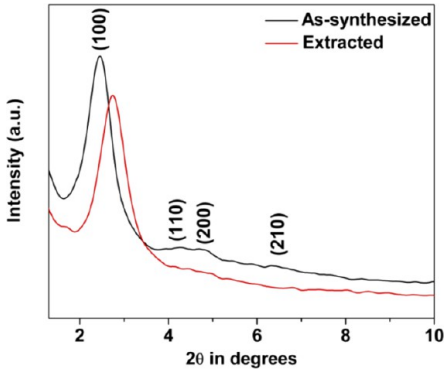

Figure 1. Small-angle X-ray diffraction pattern of PAFMS-1. The as-synthesized material is marked by a black line, and the acid-extracted material is marked by a red line.

BET Surface Area and Porosity Analysis. The porosities and surface areas of the PAFMS-1 and MCM-41 materials were estimated from the N_2 adsorption/desorption isotherms at 77 K. These isotherms are shown in Figure 2. The isotherms for PAFMS-1 can be classified as type IV corresponding to small mesopores.[49,50] If we closely analyze the isotherms for both materials (PAFMS-1 and MCM-41), then we can see that, with increasing relative pressure up to $P/P_0 > 0.2$, the amount of N_2 adsorption increases very prominently for MCM-41 and gradually for PAFMS-1, characteristic of a mesoporous material. Now, although the material (PAFMS-1) is highly ordered (observable from small-angle X-ray diffraction and TEM analysis) because of the presence of a small mesopore (2.1 nm) in the material, no sharp capillary condensation step took place at the intermediate partial pressure region (P/P_0 = 0.2−0.5), which is very much prominent in a pure MCM-41 material (pore diameter of ca. 4.2 nm).[51] The pore-size distribution of this sample was determined by employing nonlocal density functional theory (NLDFT), and this is shown in the inset of Figure 2. The BET surface area of the template-free sample is 565 $m^2\ g^{-1}$ with a pore volume of 0.2475 $cm^3\ g^{-1}$. The uniform decrease in the pore diameter (2.1 nm) and surface area of PAFMS-1 compared to the traditional MCM-41 material (surface area = 870 $m^2\ g^{-1}$; pore diameter = 4.2 nm) could be attributed to the homogeneous incorporation of a functionalized organic group bearing a phosphonic acid moiety at the surface of the ordered mesoporous channels.

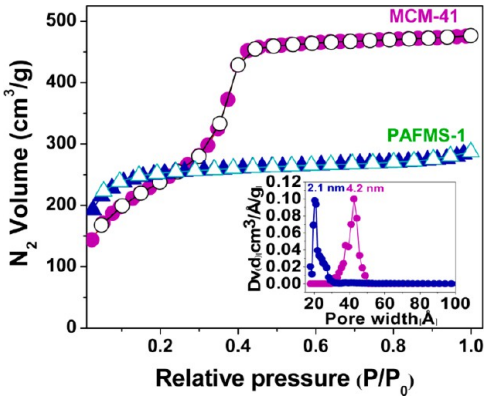

Figure 2. N_2 adsorption and desorption isotherms for PAFMS-1 and MCM-41. Adsorption points are marked by blue triangles and filled pink circles for PAFMS-1 and MCM-41, respectively. The corresponding desorption points are marked by empty triangles and empty circles, respectively. The adsorption and desorption isotherms for PAFMS-1 shifted by 100 $cm^3\ g^{-1}$. The NLDFT pore-size distribution of PAFMS-1 is shown in the inset: blue, PAFMS-1; pink, MCM-41.

Electron Microscopy Analysis. A representative HRTEM image of PAFMS-1 is shown in Figure 3a. As seen from this image, the spherical nanoparticles of the mesoporous hybrids having dimension ca. 40 nm are spread throughout the specimens similar to colloidal mesoporous silica nanoparticles.[52] A closer view of the individual nanoparticles (Figure 3b) revels that the nanoparticles are composed of honeycomb-like hexagonal arrays of pores (low-density spots in Figure 3b)

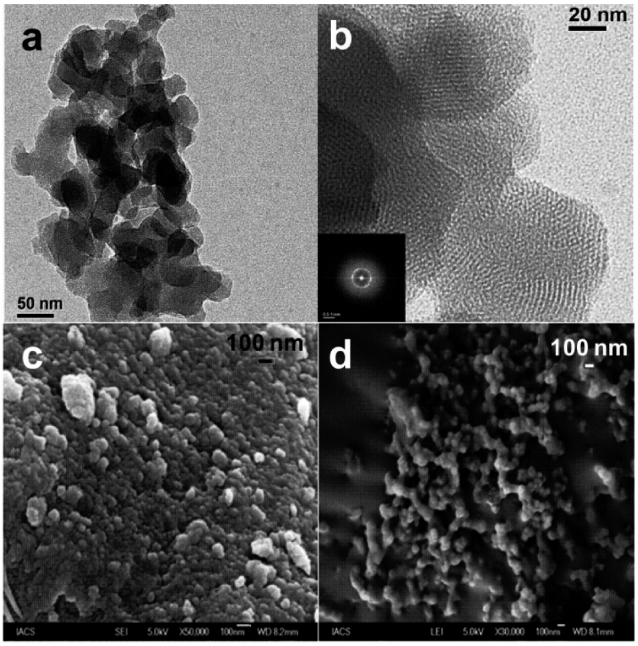

Figure 3. HRTEM images (a and b) of PAFMS-1 showing hexagonal ordering. Inset of b: FFT pattern of the material. SEM images (c and d) of the PAFMS-1 material.

dx.doi.org/10.1021/am404298a | ACS Appl. Mater. Interfaces 2014, 6, 933−941

of dimension ca. 2.1 nm. The material also showed a bright diffraction ring in the fast Fourier transform (FFT) pattern (inset of Figure 3b). Representative FESEM images of the material are shown in Figure 3c.

Further, from Figure 3d, it is evident that the material is composed of very tiny aggregated spherical nanoparticles of dimension ca. 35−40 nm. The aggregation of the spherical nanoparticles could be attributed to the strong interparticle interaction between the free surface-bound phosphonic acid groups present in the material and their self-condensation.

Solid-State MAS NMR. Solid-state CPMAS ^{13}C and MAS ^{31}P and ^{29}Si NMR experiments generally provide useful information about the chemical environment around C, P, and Si nuclei in the mesoporous hybrid PAFMS-1. The acquisition parameters of MAS ^{29}Si and ^{31}P and CPMAS ^{13}C NMR are listed in Table 1. In Figure 4, the CPMAS ^{13}C NMR

Table 1. MAS and CPMAS NMR Acquisition Parameters

		Resonance MAS			
	pulse (μs)	dwell time (μs)	acquisition time (s)	recycle delay (s)	MAS rate (kHz)
^{29}Si	2.0	14.4	0.019	5	8.0
^{31}P	4.0	5.4	0.050	5	8.0
		^{13}C CPMAS			
	$\pi/2$ pulse (μs)	dwell time (μs)	acquisition time (s)	recycle delay (s)	MAS rate (kHz)
^{13}C	5.8	13.2	0.022	5	8.0

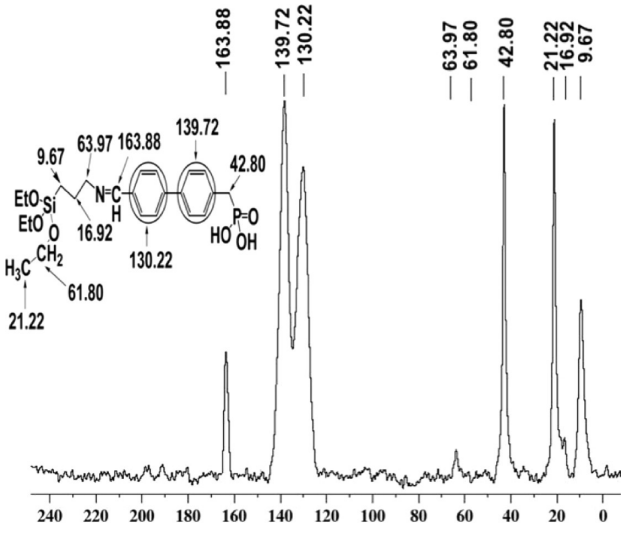

Figure 4. CPMAS ^{13}C NMR spectrum of PAFMS-1.

spectrum of PAFMS-1 is shown. The spectrum exhibits strong signals at δ 9.67, 16.92, 21.22, 42.80, 61.80, 63.97, 130.22, 139.72, and 163.88, which resemble very well the different carbon atoms of the grafted organophosphonic acid ligand in PAFMS-1 (inset of Figure 4).[53] The MAS ^{29}Si NMR spectrum (Figure 5a) of PAFMS-1 shows five peaks at ca. δ −111.32, −101.74, −91.47, −67.35, and −57.46, and these could be assigned as $Si(OSi)_4$ (Q^4), $Si(OSi)_3(OH)$ (Q^3), $Si(OSi)_2(OH)_2$ (Q^2), T^3, and T^2 bonding in the porous material.[54] The MAS ^{31}P NMR spectrum (Figure 5b) of the material shows two signals at δ 26.32 and 27.80. This can be probably be attributed to the presence of $-[P{=}(O)(OEt)_2]$ and $-[P{=}(O)(OH)(OEt)]$ in PAFMS-1.[55] The peak at δ 35.9

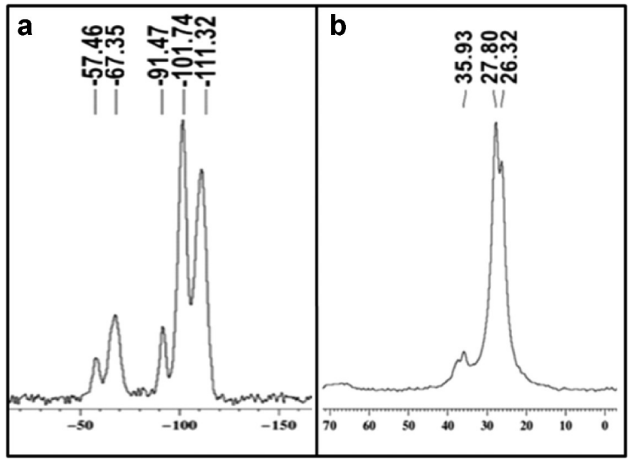

Figure 5. MAS (a) ^{29}Si and (b) ^{31}P NMR spectra of PAFMS-1.

can be attributed to the presence of free phosphonic acid $-[P{=}(O)(OH)_2]$ in the solid matrix. These results suggest that the organophosphonic acid ligand PEFOS has been covalently grafted and hydrolyzed inside the pore walls of the PAFMS-1 material.

XPS Analysis. XPS analysis was carried out to detect the presence of different framework elements and their molar ratios in PAFMS-1. The XPS spectrum of the PAFMS-1 material showed peaks for the elements carbon, phosphorus, silicon, oxygen, and nitrogen (Figure 6). This result also suggested that

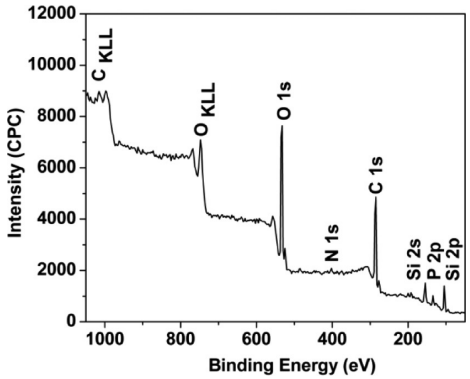

Figure 6. XPS survey curve of PAFMS-1.

the organophosphonic acid ligand was present in PAFMS-1. C 1s showed one peak with a binding energy of 285.7 eV, responsible for a sp^2-hybridized carbon atom, together with the highest energy contribution 287.5 eV, assigned to sp^3-hybridized carbon atoms in the material (Figure 7).[56] The relative amounts of two types of carbon atoms in PAFMS-1 were ca. 3.0 and 1 for $C(sp^2)$ and $C(sp^3)$, respectively, which almost exactly matched with our designed terminal PEFOS moiety after hydrolysis [$C(sp^2)/C$ (sp^3) = ca. 3.25/1]. The peak at 533 eV was responsible for ejection of an electron from O 1s of the covalently bonded oxygen atom (Figure S10 in the SI). The peak at 404 eV could be due to ejection of electrons from N 2s (Figure S11 in the SI). A broad peak at 104.4 eV could be attributed to Si 2p, which confirms the presence of a Si^{4+} oxidation state with four oxygen neighbors in PAFMS-1 (Figure S12 in the SI). The peaks at 134.6 and 191.9 eV are due to the presence of P 2p and P 2s states in PAFMS-1 (Figure S13 in the SI).[54] Elemental analysis from the XPS data

dx.doi.org/10.1021/am404298a | ACS Appl. Mater. Interfaces 2014, 6, 933−941

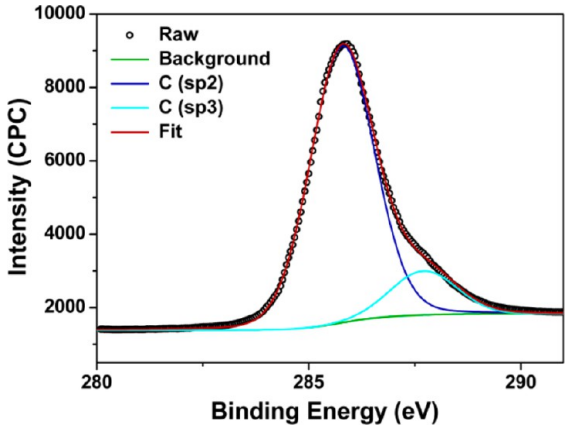

Figure 7. XPS fitting spectrum for carbon (c), showing the presence of sp^2 and sp^3 carbon atoms in the material (PAFMS-1).

suggested the presence of elements in the ratio C/O/P/N/Si = 50.51/30.96/5.64/2.54/10.35. The calculated ratio of the elements in our designed PEFOS organic scaffold after hydrolysis is C/O/P/N/Si/H = 51.64/24.28/7.83/3.54/7.10/5.51. Thus, these elemental analysis results suggested that the PEFOS moiety is covalently grafted inside the pore wall of PAFMS-1 and the phosphonate ester is hydrolyzed in the course of hydrothermal treatment and produces free phosphonic acid inside the porous channel.

FT-IR Spectroscopic Analysis. The FT-IR spectrum of PAFMS-1 showed the different framework vibrations present in the organosilane material (Figure 8). The set of bands at 952

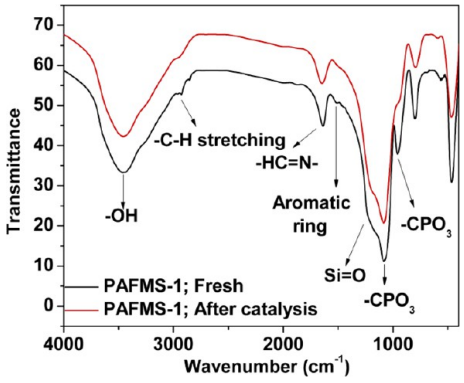

Figure 8. FT-IR spectrum of PAFMS-1.

and 1076 cm^{-1} could be assigned to the stretching vibration of a tetrahedral $-CPO_3$ group.[57] The presence of a benzene ring in the framework could be ascribed to the characteristic vibration bands at 1498 and 1605 cm^{-1}. The formation of a Schiff base (−C═N−) in the material is confirmed to be due to the presence of a sharp peak at 1636 cm^{-1}, but this peak overlapped with the physisorbed water molecule bending vibration. The small peaks centered at 2928 cm^{-1} are probably due to the stretching vibration of an alkyl C−H group in PAFMS-1. A broad band centered at 3435 cm^{-1} could be attributed to the hydroxyl (−OH) stretching vibration of hydrogen-bonded silanols in PAFMS-1.[58]

Surface Acidity via Pyridine IR. To check the nature of the surface acidity of PAFMS-1, we carried out temperature-programmable pyridine-adsorbed FT-IR spectroscopic analysis (Figure 9). The set of bands at 1630 and 1595 cm^{-1} are the

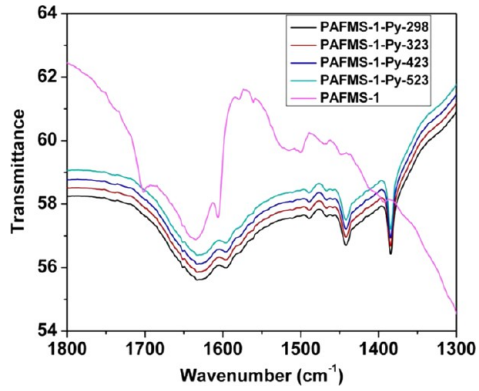

Figure 9. Temperature-programmable pyridine-adsorbed FT-IR spectra of PAFMS-1.

characteristic bands of a typical pyridinium (PyH^+) ion, confirming the presence of a Brönsted acid site in the material. This Brönsted acidity in the material is due to the free phosphonic acid [$-P(OH)_2$] in PAFMS-1. The peak at 1490 cm^{-1} confirms that pyridine is adsorbed at the same time in the Lewis and Brönsted acid sites of the material. The peak at 1442 cm^{-1} is attributed to the adsorption of pyridine to the Lewis acid side of the material. The Lewis acidity of the material is probably due to the presence of a vacant d orbital of phosphrous. A strong peak at 1384 cm^{-1} is probably due to the hydrogen-bonded pyridine (hydrogen bonding takes place with free $-P(OH)_2$) in the material. The variable-temperature FT-IR analyses at four different temperatures (298, 323, 423, and 523 K) suggested that with increasing temperature the peak intensities of the pyridine-adsorbed material decreased very slightly. This result suggested that the Brönsted acidity of the material is very strong.[59]

One-Pot Multicomponent Catalysis. The results of a one-pot three-component Biginelli condensation reaction with different substituted aldehydes, 1,3-dicarbonyl compounds, and urea/thiourea are listed in Table S1 in the SI. The yields of DHPM products are measured by weighing the yield of the final products, and these compounds are identified by ^1H and ^{13}C NMR spectroscopy. When the condensation reaction is carried out in the absence of the catalyst for 3 h at 60 °C, no desired product is identified. When the reaction is carried out over MCM-41-SO_3H as the catalyst, only 30% of the desired DHPM product is isolated. However, when we have switched over to PAFMS-1 as the catalyst in the same reaction conditions, the product yield increased to 92% (Table 2). Here the Biginelli condensation reaction may proceed through three characteristic routes: (i) enaminone formation by the aza-Michael reaction of urea with the enol form of the β-dicarbonyl compound and subsequent aldol condensation with its enamine moiety and the aldehyde followed by cyclodehydration; (ii)

Table 2. Synthesis of DHPMs in the Presence of Different Catalysts

entry	catalyst	time (h)	temperature (°C)	yield (%)
1	no catalyst	3	60	no product
2	MCM-41-SO_3H	3	60	30
3	PAFMS-1	3	60	92

[a]Reactions were carried out using benzaldehyde, ethyl acetoacetate, and urea as the reference reactant molecules.

formation of a Knovenagel adduct of the β-dicarbonyl compound and the aldehyde and subsequent aza-Michael reaction with urea by intramolecular cyclodehydration; (iii) imine or iminium intermediate formation by the reaction of aldehyde and urea, which undergo subsequent nucleophilic attack by the enol form of the β-carbonyl compound followed by intramolecular cyclocondensation.[60] To understand the possible route for the Biginelli condensation reaction, we carried out three sets of reactions with equimolar mixtures of (i) urea and ethyl acetoacetate, (ii) benzaldehyde and ethyl acetoacetate, and (iii) benzaldehyde and urea, which are heated separately at 60 °C for 3 h in the presence and absence of catalyst. In the cases of i and ii, no noticeable change was observed in the starting material after heating for 3 h at 60 °C in the presence or absence of catalyst. So, the possibility of enaminone formation and Knovenagel formation routes was ruled out. In the case of iii, a white solid product appeared after heating for 30 min at 60 °C in the absence of catalyst, and no further change of the product was observed until prolonged heating for 3 h after the addition of an equimolar amount of ethyl acetoacetate. However, in the presence of catalyst (PAFMS-1), for case iii, the white product appeared in just 10 min at 60 °C and the white product was transformed to a yellow solid product after the addition of an equimolar amount of ethyl acetoacetate, and complete product (DHPMs) transformation took place within 2−3 h.[61]

Mechanistic Pathway. We had proposed a reaction mechanism for the PAFMS-1-catalyzed Biginelli condensation reaction under solvent-free conditions in Scheme 4. The

Scheme 4. Proposed Reaction Mechanism for the Synthesis of DHPMs under PAFMS-1 as the Catalyst

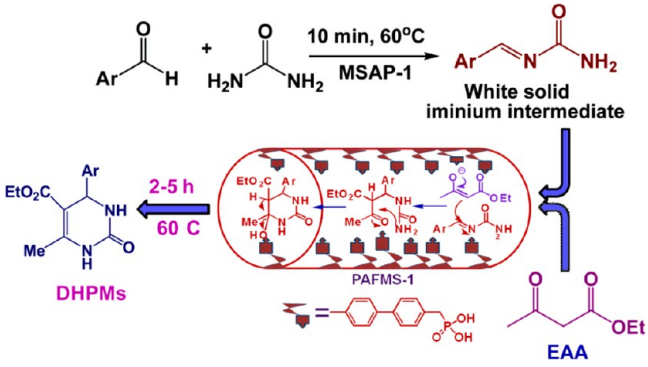

nucleophilic reaction between the iminium intermediate and the enol form of the β-dicarbonyl compound is the most crucial step for this Biginali condensation reaction. So, a highly hydrophilic porous apartment is mandatory for the incorporation of the two highly charge-separated species in this mesoporous hybrid material.[62] Along with the hydrophilic pore for suitable supramolecular assembly of the reactant molecules in the porous channel, the surface acidity of the material is also a prime factor for the nucleophilic attack and cyclocondensation reaction. So, when the condensation reaction is carried out in the presence of MCM-41-SO_3H as the catalyst, the hydrophilicity of the porous channel is not sufficient enough that it can accommodate the iminium intermediate and enol form of the β-dicarbonyl compound; however, conversion (30%) was observed because of the outer surface acidic ($-SO_3H$) group of the catalyst (MCM-41-SO_3H). However, when PAFMS-1 was used as the catalyst, containing a highly mobile π-electron system and hydrophilic phosphonic acid group in the pore wall, the prime hydrophilic reactants (iminium intermediate and enol form of the β-dicarbonyl compound) were incorporated very easily into the porous architecture and the enhanced surface acidity of the material (PAFMS-1) over MCM-41-SO_3H increased the DHPM yield to a large extent.[63] Various substituted aldehydes including electron-donating and -withdrawing groups at the different positions of the benzene ring had been employed for the one-pot three-component condensation reactions with the β-dicarbonyl compound and the urea or thiourea moiety in the presence of PAFMS-1 under solvent-free conditions. The results shown in Table 1S in the SI indicated that the nature of substitution and the position of the substituent in the aromatic ring of the aldehydes have little effect on the final yield of DHPMs. When we carried out the condensation reaction with thiourea, it took relatively more time (4.5−5 h) for completion of the reaction. This was probably due to the lower electronegativity of sulfur over oxygen, so the intermediate (arylidenethiourea) took relatively more time to introduce into the hydrophilic porous channel by enhancing the reaction time a little longer. Now, it is true that the isolated Schiff base group (−HC═N−) is very prone to hydrolysis, but here in the PAFMS-1 catalyst, the −HC═N− group remains in extensive conjugation with the biphenyl ring. Thus, the double-bond character of the imine Schiff base group is completely diminished. So, any nucleophilic attack to the imine Schiff base group of the catalyst (PAFMS-1) is largely prohibited. We monitored the FT-IR spectrum of the eight times reused catalyst (Figure 8). The FT-IR spectrum of the reused catalyst remained completely indifferent with the freshly prepared catalyst, which proved that the catalyst was stable in repeated use and the Schiff base group of PAFMS-1 did not hydrolyze during the course of the catalytic reaction.

Reusability of the Catalyst. After completion of the reaction, ethanol was added to the reaction mixture and the catalyst was recovered through filtration. Then the catalyst was washed repeatedly with methanol and acetone to remove the surface adsorbed polar and nonpolar substrates. Before the recycling test, the catalyst was dried overnight at 323 K and the procedure was repeated eight times. The reusability of the catalyst was tested with benzaldehyde, ethyl acetoacetate, and urea as the reference reactant molecules. The corresponding results are illustrated in Figure 10. The bar diagram suggests that the catalytic activity of PAFMS-1 and the surface acidity of the material (due to the presence of free phosphonic acid in PAFMS-1) did not change much after eight catalytic cycles. This result suggests high chemical stability of the phosphonic acid functionalized mesoporous material. Biginelli condensation is basically an acid-catalyzed condensation reaction, and here

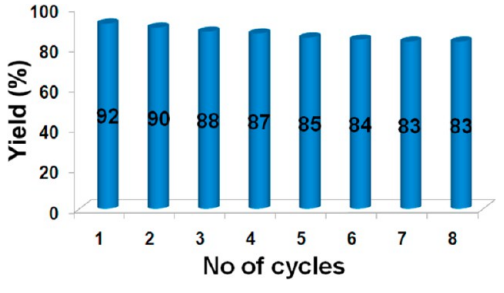

Figure 10. Recycling efficiency of the PAFMS-1 catalyst.

dx.doi.org/10.1021/am404298a | ACS Appl. Mater. Interfaces 2014, 6, 933−941

water molecules are formed as a byproduct. Probably, the product water molecules are adsorbed at the active acidic site of the catalyst, which may be responsible for very little decrease in the catalytic activity of PAFMS-1 after eight reaction cycles.

CONCLUSIONS

Here we have reported a new strategy for the synthesis of a terminal PEFOS moiety, and it has been successfully incorporated with free phosphonic acid sites in the hexagonally ordered PAFMS-1 material. The material has quite high BET surface area (565 m^2 g^{-1}) with uniform mesopores (2.1 nm). The free phosphonic acid sites together with the aromatic group present at the surface of the mesoporous material have been successfully utilized as organocatalysts for the multicomponent Biginelli reaction under solvent-free conditions for high yield and purity of the products. The experimental results suggest that the PAFMS-1 material has higher catalytic efficiency toward the condensation reaction than the MCM-41-SO_3H material. With our newly developed synthetic procedure, by tuning the primary reactant molecules, we can easily incorporate various phosphonic acid functionalized aromatics and heteroaromatics with other secondary functional groups with chirality and fluorescence properties in the porous hybrid frameworks. The strategy explored in the design of a phosphonic acid containing hexagonally ordered mesoporous material can provide new dimensions in chemical research in fields like proton-conducting materials, fluorescent markers, and heterogeneous organocatalysis.

ASSOCIATED CONTENT

Supporting Information

Table containing PAFMS-1-catalyzed DHPMS synthesis, ^1H and ^{13}C NMR of all of the products and related spectral data, XPS spectra of O 1s, N 1s, Si 2p, and P 2p of the PAFMS-1 material. This material is available free of charge via the Internet at http://pubs.acs.org.

AUTHOR INFORMATION

Corresponding Author

*E-mail: msab@iacs.res.in.

Notes

The authors declare no competing financial interest.

ACKNOWLEDGMENTS

M.P. thanks CSIR, New Delhi, India, for a senior research fellowship. A.B. thanks DST, New Delhi, India, for a DST-SERB project grant and for providing instrumental facilities through the DST Unit on Nanoscience.

REFERENCES

(1) Ramon, D. J.; Yus, M. *Angew. Chem., Int. Ed.* **2005**, *44*, 1602−1634.
(2) Denmark, S. E.; Fan, Y. *J. Am. Chem. Soc.* **2003**, *125*, 7825−7827.
(3) Cala, L.; Mendoza, A.; Fananas, F. J.; Rodrıguez, F. *Chem. Commun.* **2013**, *49*, 2715−2717.
(4) Yu, S.; You, X.; Liu, Y. *Chem.—Eur. J.* **2012**, *18*, 13936−13940.
(5) Huang, Y.; Yang, F.; Zhu, C. *J. Am. Chem. Soc.* **2005**, *127*, 16386−16387.
(6) Cohen, F.; Overman, L. E. *J. Am. Chem. Soc.* **2006**, *128*, 2594−2603.
(7) Li, N.; Chen, X. H.; Song, J.; Luo, S. W.; Fan, W.; Gong, L. Z. *J. Am. Chem. Soc.* **2009**, *131*, 15301−15310.
(8) Jain, S. L.; Singhal, S.; Sain, B. *Green Chem.* **2007**, *9*, 740−741.
(9) Atwal, K. S.; Swanson, B. N.; Unger, S. E.; Floyd, D. M.; Moreland, S.; Hedberg, A.; Reilly, B. C. O. *J. Med. Chem.* **1991**, *34*, 806−811.
(10) Yarım, M.; Sarac, S.; Ertan, M.; Batu, O.; Erol, K., II. *Farmaco* **1999**, *54*, 359−363.
(11) Sarac, S.; Yarim, M.; Ertan, M.; Boydag, S.; Erol, K. *Pharmazie* **1998**, *53*, 91−94.
(12) Barrow, J. C.; Nantermet, P. G.; Selnick, H. G.; Glass, K. L.; Rittle, K. E.; Gilbert, K. F.; Steele, T. G.; Homnick, C. F.; Freidinger, R. M.; Ransom, R. W.; Kling, P.; Reiss, D.; Broten, T. P.; Schorn, T. W.; Chang, R. S.; O'Malley, S. S.; Olah, T. V.; Ellis, J. D.; Barrish, A.; Kassahun, K.; Leppert, P.; Nagarathnam, D.; Forray, C. *J. Med. Chem.* **2000**, *43*, 2703−2718 and *61*, 1153−1162.
(13) Tawfik, H. A.; Bassyouni, F.; Gamal-Eldeen, A. M.; Abo-Zeid, M. A.; El-Hamouly, W. S. *Pharmacol. Rep.* **2009**.
(14) Tu, S.; Zhu, X.; Shi, F.; Zhang, J.; Zhang, Y. *J. Heterocycl. Chem.* **2007**, *44*, 837−842.
(15) Sachdeva, H.; Saroj, R.; Khaturia, S.; Singh, H. L. *J. Chil. Chem. Soc.* **2012**, *57*, 1012−1016.
(16) Wang, Y.; Yang, H.; Yu, J.; Miao, Z.; Chena, R. *Adv. Synth. Catal.* **2009**, *351*, 3057−3062.
(17) Ranu, B. C.; Hajra, A.; Jana, U. *J. Org. Chem.* **2000**, *65*, 6270−6272.
(18) Bhosale, R. S.; Bhosale, S. V.; Bhosale, S. V.; Wang, T.; Zubaidha, P. K. *Tetrahedron Lett.* **2004**, *45*, 9111−9113.
(19) Hankari, S. E.; Motos-Perez, B.; Hesemann, P.; Bouhaouss, A.; Moreau, J. J. E. *Chem. Commun.* **2011**, *47*, 6704−6706.
(20) Prosa, N.; Turgis, R.; Piccardi, R.; Scherrmann, M. C. *Eur. J. Org. Chem.* **2012**, 2188−2200.
(21) Sharma, S. D.; Gogoi, P.; Konwar, D. *Green Chem.* **2007**, *9*, 153−157.
(22) Gholap, A. R.; Venkatesan, K.; Daniel, T.; Lahoti, R. J.; Srinivasan, K. V. *Green Chem.* **2004**, *6*, 147−150.
(23) Weiss, C. J.; Marks, T. J. *Dalton Trans.* **2010**, *39*, 6576−6588.
(24) Metz, M. V.; Schwartz, D. J.; Stern, C. L.; Nickias, P. N.; Marks, T. J. *Angew. Chem., Int. Ed.* **2000**, *39*, 1312−1316.
(25) Bellis, E.; Kokotos, G. *J. Mol. Catal., A: Chem.* **2005**, *241*, 166−174.
(26) Aguirre, M. R.; Saenz, L. D. L. T.; Flores, W. A.; Sanchez, A. R.; Elguezabal, A. A. *Catal. Today* **2005**, *107*, 310−314.
(27) Kim, H. S.; Song, Y. M.; Choi, J. S.; Yang, J. W.; Han, H. *Tetrahedron* **2004**, *60*, 12051−12057.
(28) Pereza, B. M.; Roeserb, J.; Thomasb, A.; Hesemanna, P. *Appl. Organomet. Chem.* **2013**, *27*, 290−299.
(29) Merino, E.; Sesto, E. V.; Maya, E. M.; Iglesias, M.; Sanchez, F.; Corma, A. *Chem. Mater.* **2013**, *25*, 981−988.
(30) Comotti, A.; Bracco, S.; Valsesia, P.; Ferretti, L.; Sozzani, P. *J. Am. Chem. Soc.* **2007**, *129*, 8566−8576.
(31) Yamauchi, Y.; Suzuki, N.; Gupta, P.; Sato, K.; Fukata, N.; Murakami, M.; Shimizu, T.; Inoue, T.; Kimura, T. *Sci. Technol. Adv. Mater.* **2009**, *10*, 025005.
(32) Sharifi, M.; Kohler, C.; Tolle, P.; Frauenheim, T.; Wark, M. *Small* **2011**, *7*, 1086−1097.
(33) Lebed, P. J.; Savoie, J. D.; Florek, J.; Bilodeau, F.; Lariviere, D.; Kleitz, F. *Chem. Mater.* **2012**, *24*, 4166−4176.
(34) Mizoshita, N.; Yamanaka, K. I.; Hiroto, S.; Shinokubo, H.; Tani, T.; Inagaki, S. *Langmuir* **2012**, *28*, 3987−3994.
(35) Brunelli, N. A.; Venkatasubbaiah, K.; Jones, C. W. *Chem. Mater.* **2012**, *24*, 2433−2442.
(36) Liu, K.; Jin, R.; Cheng, T.; Xu, X.; Gao, F.; Liu, G.; Li, H. *Chem.—Eur. J.* **2012**, *18*, 15546−15553.
(37) Sasidharan, M.; Bhaumik, A. *ACS Appl. Mater. Interfaces* **2013**, *5*, 2618−2625.
(38) Nandi, M.; Mondal, J.; Sarkar, K.; Yamauchi, Y.; Bhaumik, A. *Chem. Commun.* **2011**, *47*, 6677−6679.
(39) Jain, S. L.; Modak, A.; Bhaumik, A. *Green Chem.* **2011**, *13*, 586−590.
(40) Suzuki, N.; Gupta, P.; Sukegawa, H.; Inomata, K.; Inoue, S.; Yamauchi, Y. *J. Nanosci. Nanotechnol.* **2010**, *10*, 6612−6617.

(41) Suzuki, N.; Yamauchi, Y. *J. Nanosci. Nanotechnol.* **2010**, *10*, 5759−5766.
(42) Yamauchi, Y.; Suzuki, N.; Sato, K.; Fukata, N.; Murakami, M.; Shimizu, T. *Bull. Chem. Soc. Jpn.* **2009**, *82*, 1039−1043.
(43) Alvim, H. G. O.; de Lima, T. B.; de Oliveira, H. C. B.; Gozzo, F. C.; de Macedo, J. L.; Abdenur, P. V.; Silva, W. A.; Neto, B. A. D. *ACS Catal.* **2013**, *3*, 1420−1430.
(44) Shiri, M. *Chem. Rev.* **2012**, *112*, 3508−3549.
(45) Yamauchi, Y.; Suzuki, N.; Radhakrishnan, L.; Wang, L. *Chem. Rec.* **2009**, *9*, 321−339.
(46) Yamauchi, Y. J. *Ceram. Soc. Jpn.* **2013**, *121*, 831−840.
(47) Lee, H. I.; Kim, J. M.; Stucky, G. D. *J. Am. Chem. Soc.* **2009**, *131*, 14249−14251.
(48) Kleitz, F.; Schmidt, W.; Schuth, F. *Microporous Mesoporous Mater.* **2003**, *65*, 1−29.
(49) Cychosz, K. A.; Guo, X.; Fan, W.; Cimino, R.; Gor, G. Y.; Tsapatsis, M.; Neimark, A. V.; Thommes, M. *Langmuir* **2012**, *28*, 12647−12654.
(50) Savithra, G. H. L.; Bowker, R. H.; Carrillo, B. A.; Bussell, M. E.; Brock, S. L. *ACS Appl. Mater. Interfaces* **2013**, *5*, 5403−5407.
(51) Kruk, M.; Jaroniec, M. *Chem. Mater.* **2001**, *13*, 3169−3183.
(52) Yamada, H.; Urata, C.; Aoyama, Y.; Osada, S.; Yamauchi, Y.; Kuroda, K. *Chem. Mater.* **2012**, *24*, 1462−1471.
(53) Modak, A.; Mondal, J.; Aswal, V. K.; Bhaumik, A. *J. Mater. Chem.* **2010**, *20*, 8099−8106.
(54) Chandra, D.; Yokoi, T.; Tatsumi, T.; Bhaumik, A. *Chem. Mater.* **2007**, *19*, 5347−5354.
(55) Pramanik, M.; Nandi, M.; Uyama, H.; Bhaumik, A. *Catal. Sci. Technol.* **2012**, *2*, 613−620.
(56) Vinu, A.; Ariga, K.; Mori, T.; Nakanishi, T.; Hishita, S.; Golberg, D.; Bando, Y. *Adv. Mater.* **2005**, *17*, 1648−1652.
(57) Lu, J.; Li, Y.; Deng, C. *Nanoscale* **2011**, *3*, 1225−1233.
(58) Borah, P.; Ma, X.; Nguyen, K. T.; Zhao, Y. *Angew. Chem., Int. Ed.* **2012**, *51*, 7756−7761.
(59) De, S.; Dutta, S.; Patra, A. K.; Rana, B. S.; Sinha, A. K.; Saha, B.; Bhaumik, A. *Appl. Catal., A* **2012**, *435*, 197−203.
(60) Roy, S. P.; Jadhavar, P. S.; Seth, K.; Sharma, K. K.; Chakraborti, A. K. *Synthesis* **2011**, *14*, 2261−2267.
(61) De Souza, R. O. M. A.; Penha, E. T. D.; Milagre, H. M. S.; Garden, S. J.; Esteves, P. M.; Eberlin, M. N.; Antunes, O. A. C. *Chem.—Eur. J.* **2009**, *15*, 9799−9804.
(62) Tayebeea, R.; Aminib, M. M.; Ghadamgahia, M.; Armaghan, M. *J. Mol. Catal., A: Chem.* **2013**, *366*, 266−274.
(63) Karimi, B.; Mirzaei, H. M.; Mobaraki, A. *Catal. Sci. Technol.* **2012**, *2*, 828−834.